THE ASTROPHYSICAL JOURNAL, 363:515–527, 1990 November 10

FARADAY ROTATION MEASURE VARIATIONS IN THE CYGNUS REGION AND THE SPECTRUM OF INTERSTELLAR PLASMA TURBULENCE

T. JOSEPH LAZIO AND STEVEN R. SPANGLER
Department of Physics and Astronomy, University of Iowa

AND

JAMES M. CORDES
Department of Astronomy and National Astronomy and Ionosphere Center, Cornell University
Received 1989 July 31; accepted 1990 April 11

ABSTRACT

Linear polarization observations were made of eight double-lobed radio galaxies viewed through the galactic plane in the Cygnus region. These observations have been used to determine intra- and intersource rotation measure differences; in some cases, we have extracted unambiguous rotation measures. The rotation measures are dominated by foreground magnetoionic material. The differences in rotation measure between pairs of sources correlate with angular separation for separations from 10″ to 1°.5. These rotation measure fluctuations are consistent with a model in which the electron density varies on ≈ 0.1–200 pc scales. The amplitudes of these variations are, in turn, consistent with those electron density variations that cause diffractive interstellar scattering on scales less than 10^{11} cm.

Subject headings: interstellar: magnetic fields — polarization — turbulence

I. INTRODUCTION

In the past few years there has been considerable progress in the subject of radio wave scattering in the interstellar medium. A recent and comprehensive summary of activity in this field is given in Cordes, Rickett, and Backer (1988).

In spite of improved observational specification of the phenomena, there remains almost complete uncertainty regarding the physical nature of the density irregularities responsible for interstellar scattering. Suggestions have been made that the irregularities are nonpropagating entropy structures analogous to those seen in hydrodynamic turbulence (Higdon 1984, 1986), analogous to Lighthill radiation in magnetohydrodynamic turbulence (Montgomery, Brown, and Mattaeus 1987), or the compressive component of magnetohydrodynamic waves (Spangler *et al.* 1986; Spangler 1988).

The attempt to decide between these suggestions would be considerably assisted by furthering our knowledge in two areas. First, we need to know the form of the spatial spectrum over a wide range of wavenumbers. It has previously been suggested by Lee and Jokipii (1976) and Armstrong, Cordes, and Rickett (1981) that the density power spectrum is a power law which extends to an outer scale on the order of parsecs. For a power-law spatial spectrum $P_{\delta n}(q) = C_n^2 q^{-\alpha}$ with $\alpha < 4$, most observables tend to be dominated by small-scale irregularities and are much less sensitive to large-scale variations. Diffractive phenomena, such as angular broadening of radio sources and pulse broadening of pulsars, provide measurements of the density irregularities on scales of 10^8–10^{10} cm, but are relatively insensitive to irregularities on much larger scales. Thus, the outer scale of the turbulence (defined as the reciprocal of the smallest wavenumber for which the spectrum is a power law) may be $\approx 10^{12}$ cm or much larger. Second, there is a need to know the relationship between the density perturbations which produce scattering, and the (presumably) associated magnetic field variation. In this paper, we report observations which should contribute to both of these presently poorly known topics.

To study interstellar turbulence, we make use of the Faraday rotation measure and its structure function. Linearly polarized radiation passing through a magnetized plasma experiences a rotation of the polarization position angle. The polarization position angle upon emergence from the plasma is given by

$$\phi = \phi_0 + \mathrm{RM}\ \lambda^2 , \tag{1}$$

where ϕ_0 is the initial polarization position angle of the radiation before it enters the plasma, λ is the wavelength, and RM is the Faraday rotation measure, given by

$$\mathrm{RM} = \frac{e^3}{2\pi m^2 c^2} \int_L n_e \boldsymbol{B} \cdot d\boldsymbol{l} , \tag{2}$$

where e is the charge on the electron, m is the mass of the electron, c is the speed of light, n_e is the electron density, $\boldsymbol{B}$ is the magnetic field, and L is the path length.

Differences in the rotation measure along two different lines of sight may be quantitatively studied with the structure function, $D_{\mathrm{RM}}(\Delta\theta)$. The structure function contains information on the statistics of the RM variations and ultimately is determined by the nature of the plasma turbulence in the interstellar medium. The structure function is defined by

$$D_{\mathrm{RM}}(\Delta\theta) \equiv \langle [\mathrm{RM}(\theta) - \mathrm{RM}(\theta + \Delta\theta)]^2 \rangle , \tag{3}$$

where angle brackets indicate an expectation value. In writing equation (3), we have assumed that the statistics of the RM fluctuations are stationary, i.e., not dependent on θ, and isotropic, or dependent only on the magnitude of $\Delta\theta$ and not its orientation.

In this paper, we report linear polarization measurements, yielding Faraday rotation measures, for eight double radio galaxies in the galactic plane in the vicinity of Cygnus. This region of the sky was chosen because our previous observations (Spangler *et al.* 1986; Fey, Spangler, and Mutel 1989) have measured the interstellar scattering on a number of lines of sight, and other observations (Spangler and Cordes 1988)

have measured the spectrum of the density turbulence. The scattering in this direction is also quite heavy, indicating that lines of sight through the Galaxy have encountered one or more of the intense scattering clumps referred to by Dennison *et al.* (1984) and Cordes, Weisberg, and Boriakoff (1985). Observations in the Cygnus region, therefore, permit us to investigate highly scattered lines of sight for which the small-scale density irregularities are well-specified.

Sources in this part of the sky are viewed through a complex of OB associations, stellar wind sources, and supernova remnants referred to as the "Cygnus superbubble" (Bochkarev and Sitnik 1985). Although many of the objects and associations are not spatially contiguous, appearing together on the sky only through projection effects, lines of sight passing through the superbubble nevertheless encounter a number of distinct objects. Most of the objects in the superbubble are believed to be between 0.5 and 2.5 kpc distant (Bochkarev and Sitnik 1985).

In § II we describe the observations and preliminary data reduction, in § III we present the observational results, in § IV we describe the extraction of polarization position angles and determination of the rotation measures of the sources, in § V we form the structure function and compare it with a simple model, and in § VI we summarize our results.

II. OBSERVATIONS

The observations occurred over a 3 yr period. In the summer of 1985, a region of roughly 10 deg^2 centered on the source 2013+370 was surveyed with the VLA[1] at 1.46 GHz. Follow-up observations of discrete sources were made a few weeks later at 5 GHz. These observations were motivated by the observation of interstellar scattering of 2013+370 (Spangler *et al.* 1986) and the desire to discover additional compact extragalactic sources in the vicinity, which could be used to map the distribution of scattering in this region. These observations also revealed eight objects which we identified as extended extragalactic radio sources. Seven of the eight sources showed characteristic double structure. The locations of these eight sources are shown in Figure 1. Since extended extragalactic radio sources are typically linearly polarized, we decided that these would be good objects for Faraday rotation measurements.

The first set of polarimetric observations was made on 1987 January 18, when the VLA was in the C-array. Full polarimetric data were obtained in two contiguous 50 MHz bandpasses centered at 4835 and 4885 MHz. Observations were made over a 12 hr period, and each source was observed at 5 hour angles. At each hour angle, 15 minutes of integration were obtained.

The second set of observations was obtained on 1988 January 31 and February 1 at L band with the VLA in the B-array. The use of the VLA in this scaled array permitted the same spatial frequencies to be sampled as in the C band observations. The AC and BD correlators were split for these observations with the AC pair being set at 1437.5 MHz and the BD pair at 1652.5 MHz. The bandwidth at both L band frequencies was 25 MHz. Like the C band observations, the L band observations were also made over a 12 hr period with each source being observed at 5 hour angles and 15 minutes of integration time being obtained at each hour angle.

After correcting for instrumental polarization, corrections were applied to the L band data for ionospheric Faraday rotation. The corrections were initially applied at the VLA site using the ionospheric electron density values from 1986 January. These electron density values were judged to be the most representative of the past several years for the observing conditions encountered. After the 1988 January electron density values became available, the phase corrections were calculated again. In both cases, the magnitude of these phase corrections was small, ranging from 0° to 8°. As the difference between the two corrections was small, never more than 2° of phase, it was decided not to recalibrate the data, but leave the corrections applied with the 1986 January electron density values.

Using the NRAO Astronomical Image Processing System, maps of the Stokes I, Q, and U parameters were produced. For a given source, the restoring beam used to generate the CLEANed I, Q, and U maps was the same at all frequencies. For all sources, the restoring beam was approximately 4″ by 4″. The Q and U images were combined to form the linear polarization intensity image, $L \equiv \sqrt{Q^2 + U^2}$, and the polarization position angle image, $\phi \equiv \frac{1}{2} \arctan (U/Q)$. An image of another common polarization observable, the degree of linear polarization, $m \equiv L/I$, was also formed.

In Table 1 we display the positions and measured fluxes (Stokes parameter I) of these sources. In column (1) is the source name, column (2) designates the strongest component of the source, columns (3) and (4) display the equatorial coordinates of the most intense feature within the component of column (2), and columns (5), (6), and (7) show the integrated flux density of the source at the frequencies 1437.5, 1652.5, and 4885 MHz, respectively. We do not list here the measured flux of the sources at 4835 MHz.

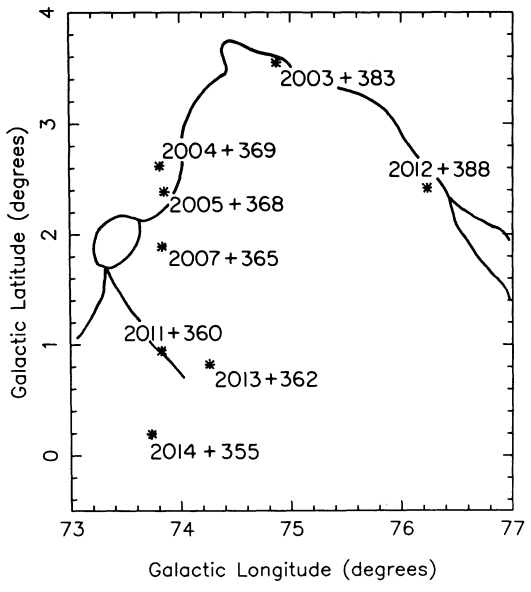

FIG. 1.—The positions of the eight extragalactic sources displayed as a function of galactic latitude and longitude. Dark curve marks the most intense optical emission from the Cygnus loop as it appears on the Palomar Sky Survey print.

[1] The Very Large Array is a part of the National Radio Astronomy Observatory operated by Associated Universities, Inc., under contract with the National Science Foundation.

TABLE 1

SOURCE POSITIONS AND FLUX DENSITIES

SOURCE	COMPONENT	α	δ	S_ν (mJy) 1438 MHz	1652 MHz	4885 MHz
2003+383.....	SP	$20^h\ 3^m40^s.557$	38°18′48″.63	113.10	90.78	33.22
2004+369.....	NP	20 4 41.583	36 55 7.71	122.33	102.45	50.18
2005+368.....	NP	20 5 47.436	36 50 0.71	560.30	497.41	176.60
2007+365.....	SF	20 7 46.617	36 32 10.50	77.87	75.12	33.18
2011+360.....	SP	20 11 41.484	36 0 17.60	276.40	236.63	98.55
2012+388.....	SP	20 12 20.842	38 49 23.61	59.65	60.63	25.74
2013+362.....	SP	20 13 23.681	36 17 44.50	503.71	462.04	164.74
2014+355.....	SF	20 14 27.450	35 30 26.40	178.37	134.97	48.10

III. OBSERVATIONAL RESULTS

We present maps of the sources at three frequencies: 1437.5 MHz, 1652.5 MHz, and 4885 MHz. The format for Figure 2 is the following. For each source, there is a total intensity contour image at 4885 MHz and images of the polarization position angle at the three frequencies. The vectors are oriented as the polarization position angles and their lengths are proportional to the polarized intensity. A low contour marks the boundary of the source. Displayed in Table 2 are the intensities and angles measured for the principal components of each source. Column (1) gives the source name, and column (2) is the component designation in conventional "north-preceding, south-following" notation. The frequency of observation is given in column (3); we do not list here separate data for the other C band channel. Columns (4) and (5) list, respectively, the peak total and polarized intensity for the component. Columns (6) and (7) give the polarization position angle of the component as determined in two different ways. In column (6) we present the spatial average of the polarization position angle over the component, while in column (7) we give the polarization position angle at the position in the component where the polarized intensity is highest. We refer to these two methods as spatial averaging and single feature, respectively. For most components, the polarized emission was only slightly resolved or showed only small spatial gradients; consequently, the polarization position angles determined in these two methods are generally the same.

The errors in these polarization position angle measurements, given in parentheses, also deserve comment. In the case of the spatial average of the polarization position angle, $\bar{\phi}$, the error was calculated from the internal dispersion of the pixel values in the region over which the average was taken. For the polarization position angle of the most highly polarized feature, $\phi_{\rm peak}$, the uncertainty was calculated from the theory of errors in polarimetric observables (e.g., Rankin, Campbell, and Spangler 1975). Such a calculation requires knowledge of the errors in Q and U, σ, which were assumed and in practice found to be equal. We measured these by taking the rms noise in the Q and U maps on a blank portion of the map far from the source.

An additional important quantity which may be calculated from the data in Table 2 is the depolarization, or ratio of fractional linear polarization at a lower frequency to that at a higher frequency. This quantity is of interest because it is a crude indicator of internal Faraday rotation and may, furthermore, be used to limit the Faraday rotation through the phenomenon of bandwidth depolarization. Further and quantitative discussion of this matter is given in § IV.

Additional discussion of each source is deferred until the rotation measures have been presented.

IV. DATA REDUCTION AND ANALYSIS

a) Extraction of Polarization Position Angles

As mentioned in § III, two methods were used to extract polarization position angles for source components. We now wish to discuss these two methods further, and particularly their relative advantages and disadvantages.

The principal advantage of the spatial averaging method is that it yields a "global" value of the polarization position angle, i.e. one obtained from a larger volume of the source. We would expect it to be less susceptible to depolarization effects which can shift the location of polarized structure at different frequencies.

One disadvantage of this method is its sensitivity to spatial gradients in the polarization position angle at each frequency. This should not affect the mean value of the polarization position angle provided that, as was done, the average at all frequencies is calculated over exactly the same part of the source. However, structural variations in the polarization position angle will also inflate errors assigned to the measurement, since these structural changes will be added to the truly random noise contributions.

In an attempt to minimize this effect, we computed the average over the largest region for which the polarization position angle was relatively uniform. The implementation of this practice is illustrated by 2005+368. As can be seen in Figure 2*c*, the polarization structure in the south-following component consists of two "domains" at the two lower frequencies, whereas only one of these (the southernmost) is identified as a region of uniform polarization position angle at 4885 MHz. The integration was confined to this southernmost feature.

The principal disadvantage to these spatially averaged polarization position angles is that they are nonoptimum from the viewpoint of signal-to-noise ratio. In forming this polarization position angle estimate, we average regions of high and low signal-to-noise ratio, thereby increasing the error in the extracted polarization position angle. As will be seen § IV*b* below, this larger error allows more values for the rotation measure to be permissible in a least-squares sense.

The second method, choosing only the brightest polarization feature, is based on the notion that random errors of the most intense feature would be smaller than that of a spatial average. The errors in this second method were determined from the signal-to-noise ratio. If the polarized intensity at the location of interest is L and the rms noise in the Stokes Q or U

image is σ, then the error in the polarization position angle is $\sigma_\phi = \frac{1}{2}(\sigma/L)$, for $\sigma \ll L$.

There are two difficulties with this method. First, there is the danger that depolarization would depend on location in the source, i.e., depolarization would cause the position of peak polarized intensity to be different at L band and C band. This situation could then result in the polarization position angle measurements at different frequencies referring to different positions. Although checks on the spatial coincidence of features of interest indicated that the aforementioned effect was not present at a significant level, this remains a possible source of error.

The second difficulty is that this method will tend to underestimate σ, and therefore σ_ϕ. Our measurement of σ comes

TABLE 2

SOURCE PARAMETERS

Source	Component[a]	ν (MHz)	I_{max} (mJy beam^{-1})	L_{max} (mJy beam^{-1})	$\bar{\phi}$[b]	ϕ_{peak}[b]
2003+383.....	SP	1438	64.12	1.07	85°0(7°0)	78°4 (5°8)
		1652	54.81	1.26	68.9(3.5)	66.3 (3.8)
		4885	18.58	1.59	93.1(3.5)	94.7 (1.6)
	NF	1438	26.00	0.96	142.1(13)	138.6 (4.1)
		1652	21.44	0.85	149.5(3.5)	150.9 (6.1)
		4885	6.83	0.50	124.4(8.4)	120.4 (5.2)
2004+369.....	NP	1438	41.12	1.52	145 (37)	139.6 (2.1)
		1652	37.38	1.96	1 (37)	2.1 (1.7)
		4885	16.74	1.07	50 (28)	60.4 (2.6)
	SF	1438	40.13	1.10	113 (16)	106.8 (2.9)
		1652	35.28	0.88	129 (19)	133.0 (3.9)
		4885	14.05	0.68	147.9(6.9)	150.2 (4.1)
2005+368.....	NP	1438	210.25	6.24	159.9(9.9)	153.85(0.57)
		1652	185.95	6.26	95.5(5.6)	92.56(0.59)
		4885	65.04	2.47	17.7(5.2)	16.0 (1.2)
	SF	1438	205.27	5.82	1.2(5.7)	0.62(0.62)
		1652	183.15	5.26	128.8(7.5)	125.37(0.75)
		4885	64.98	2.50	56 (22)	49.1 (1.2)
2007+365.....	NP	1438	10.90	3.22	70.2(1.5)	71.1 (1.0)
		1652	10.47	3.18	81.3(4.2)	81.5 (1.0)
		4885	4.53	1.30	161.4(9.5)	158.9 (2.7)
	SF	1438	18.37	4.52	102.7(5.2)	100.22(0.74)
		1652	16.73	4.14	74.6(7.8)	75.43(0.81)
		4885	7.39	1.78	58.2(6.8)	58.0 (2.0)
2011+360.....	SP	1438	89.85	2.39	167 (13)	154.8 (3.5)
		1652	80.82	2.63	32 (16)	9.9 (2.2)
		4885	32.26	1.51	146 (3.6)	163.6 (1.7)
	NF	1438	17.53	1.44		91.0 (2.4)
		1652	16.06	1.43		69.3 (2.5)
		4885	5.94	0.67		46.7 (4.4)
2012+388[c].....	SP	1438	4.98	0.31	...	...
		1652	4.69	0.21	...	...
		4885	7.07	0.82	52.7(9.5)	52.2 (3.2)
	NF	1438	0.31	0.33	...	...
		1652	0.21	0.21	...	...
		4885	4.21	0.50	90 (12)	81.4 (6.2)
2013+362.....	SP	1438	190.39	1.55	32 (12)	35.8 (2.3)
		1652	172.36	2.45	34 (12)	38.6 (1.5)
		4885	62.13	4.84	76.0(6.9)	71.38(0.52)
	NF	1438	173.64	6.08	32.6(6.4)	35.13(0.56)
		1652	159.78	9.12	8.6(4.9)	11.40(0.40)
		4885	62.67	8.73	151.9(7.6)	149.76(0.31)
2014+355[d].....	NP, hot spot	1438	26.84	2.69	81 (21)	81.4 (1.3)
		1652	23.36	2.71	93 (23)	90.7 (1.3)
		4885	8.00	0.91	77 (25)	71.8 (2.9)
	NP, lobe	1438	8.84	2.27		32.5 (1.5)
		1652	6.31	1.83		39.9 (2.0)
		4885	1.99	0.58		12.9 (4.6)
	SF, hot spot	1438	42.93	7.85	66.7(7.9)	64.70(0.43)
		1652	38.84	7.77	45.6(5.5)	45.31(0.47)
		4885	14.48	3.17	120.7(6.1)	124.19(0.84)
	SF, lobe	1438	15.95	2.95	106.9(9.7)	108.7 (1.2)
		1652	13.32	2.52	85.1(5.6)	88.4 (1.5)
		4885	2.67	0.67	176 (20)	1.3 (4.0)

[a] An "N" or "S" indicates North and South, respectively. A "P" or "F" indicates preceding and following, respectively.

[b] Numbers in parentheses are errors.

[c] A dash (–) indicates no measurement possible due to lack of polarized intensity.

[d] For 2014+355, the hot spots are the regions of the highest total intensity and the lobes are outlying regions.

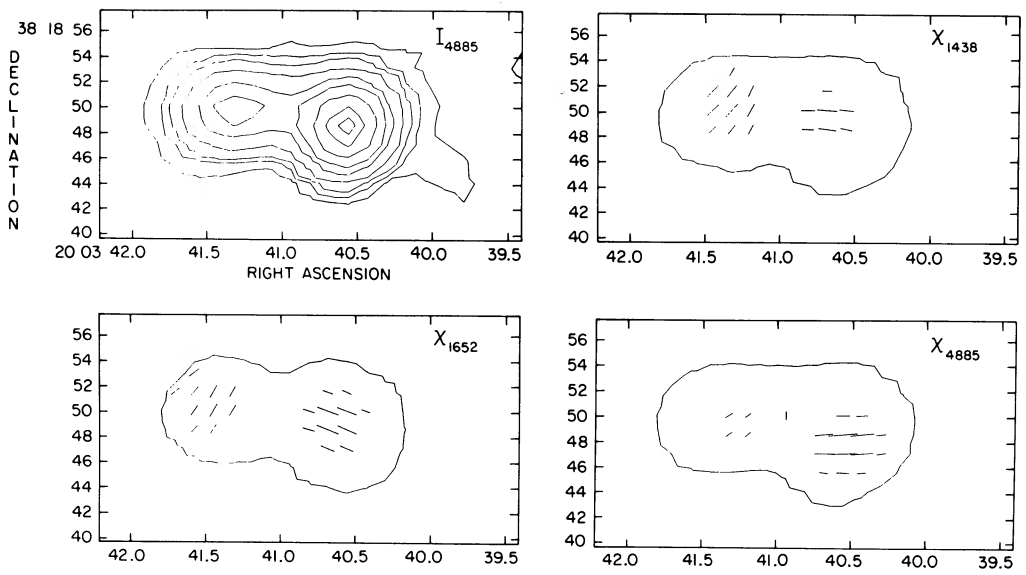

FIG. 2a

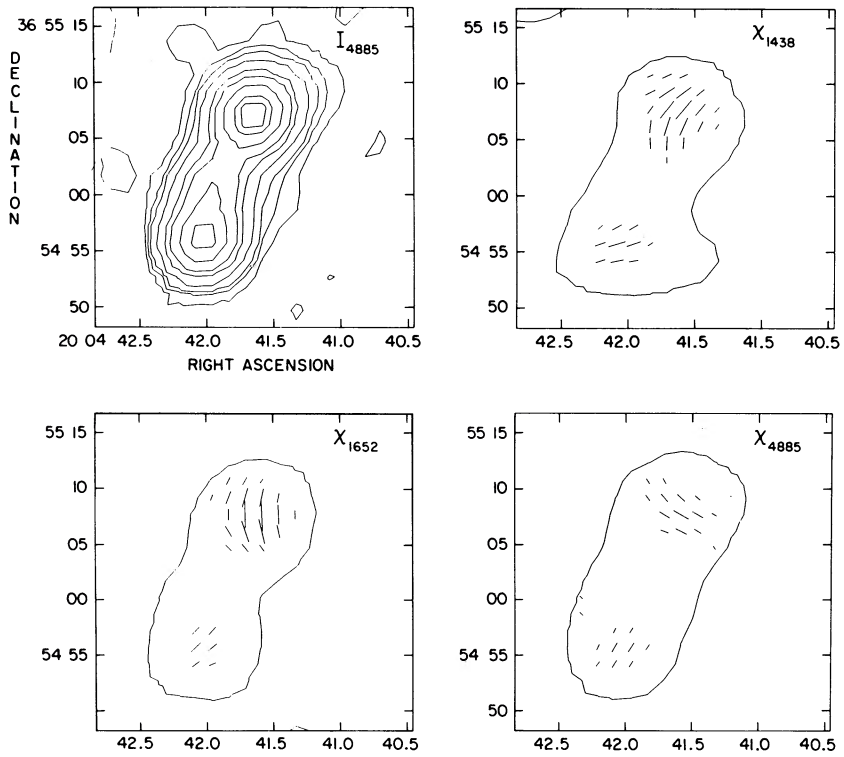

FIG. 2b

FIG. 2.—(*a*) Maps of the source 2003+383 are displayed. In the upper left panel is a total intensity contour image. Contours are 0.01, 0.03, 0.05, 0.10, 0.20, 0.30, 0.50, 0.75, and 0.90 of the peak intensity. The remaining three panels show the polarization position angles at 1438, 1652, and 4885 MHz. The position angles of the vectors are that of the polarization position angles, and the lengths of the vectors are proportional to the polarized intensity. A low contour marks the boundary of the source. (*b*) Same as (*a*), except for 2004+369. (*c*) Same as (*a*), except for 2005+368. (*d*) Same as (*a*), except for 2007+365. Contours are 0.03, 0.05, 0.10, 0.20, 0.30, 0.50, 0.75, and 0.90. (*e*) Same as (*d*), except for 2011+360. (*f*) Maps of the source 2012+388 are displayed. In the left panel is a total intensity contour image. Contours are 0.03, 0.05, 0.10, 0.20, 0.30, 0.50, 0.75, and 0.90 of the peak intensity. The right panel shows the polarization position angles at 4885 MHz. As this source was unpolarized at the two lower frequencies, images at these frequencies are not shown. (*g*) Same as (*a*), except for 2013+362. (*h*) Same as (*d*), except for 2014+355.

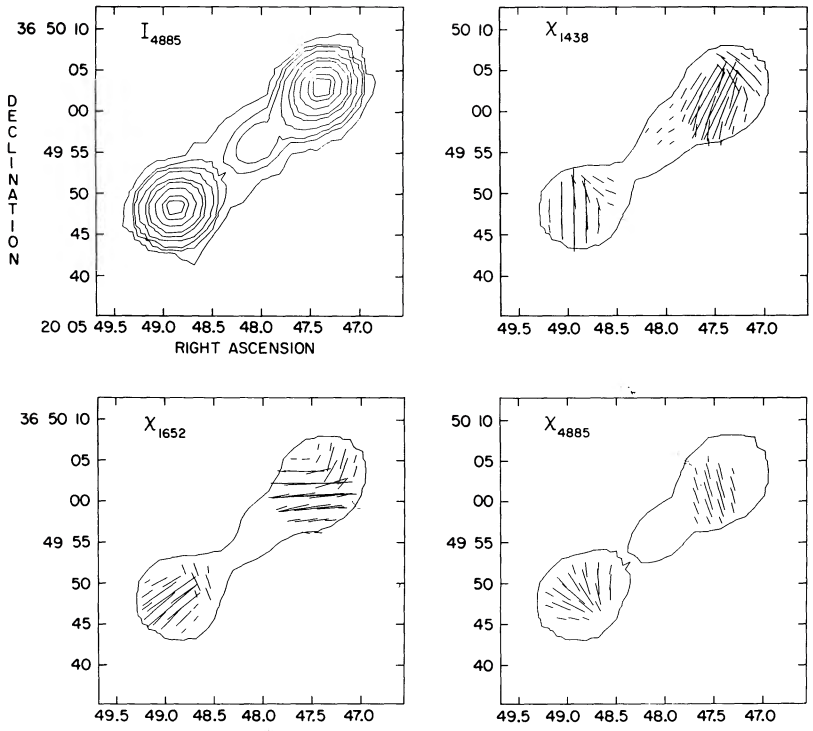

FIG. 2c

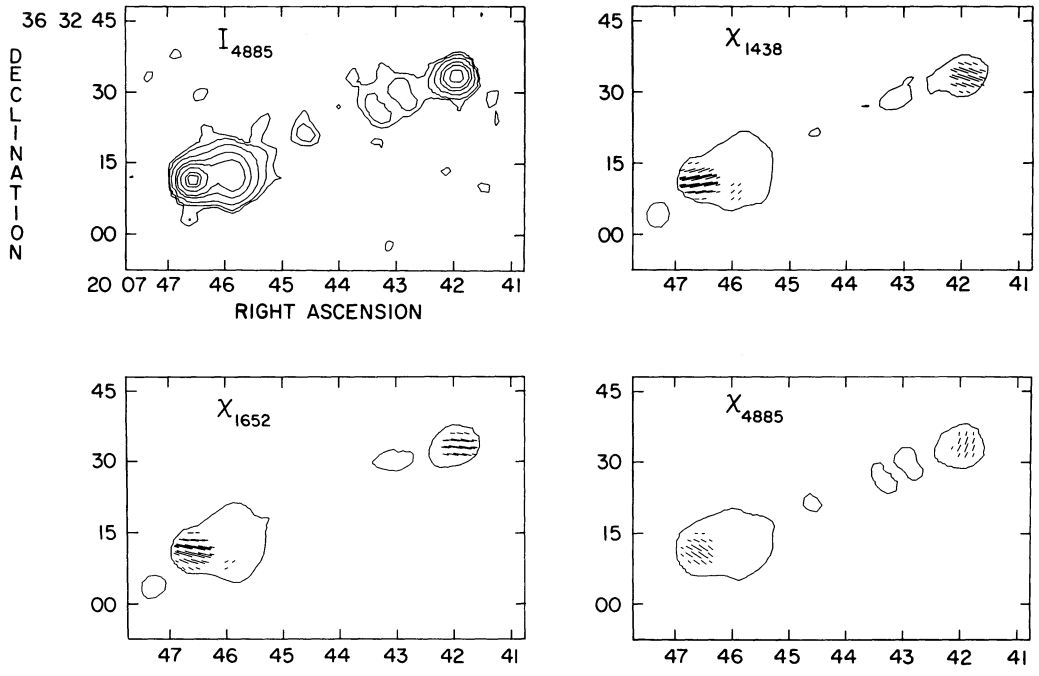

FIG. 2d

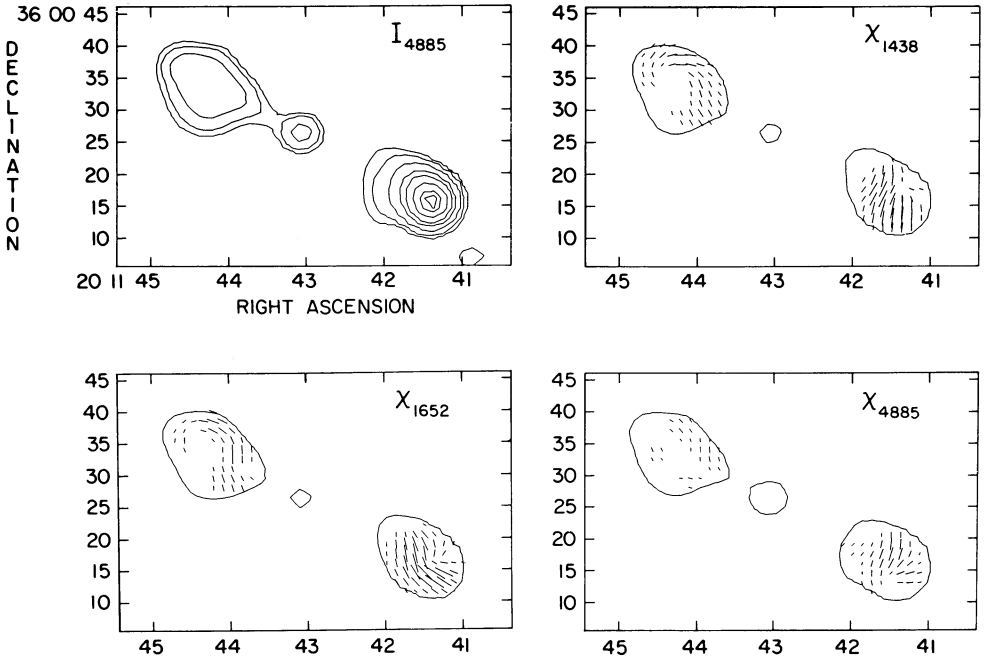

FIG. 2e

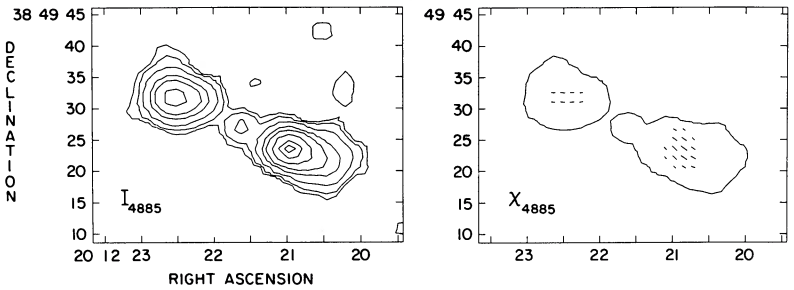

FIG. 2f

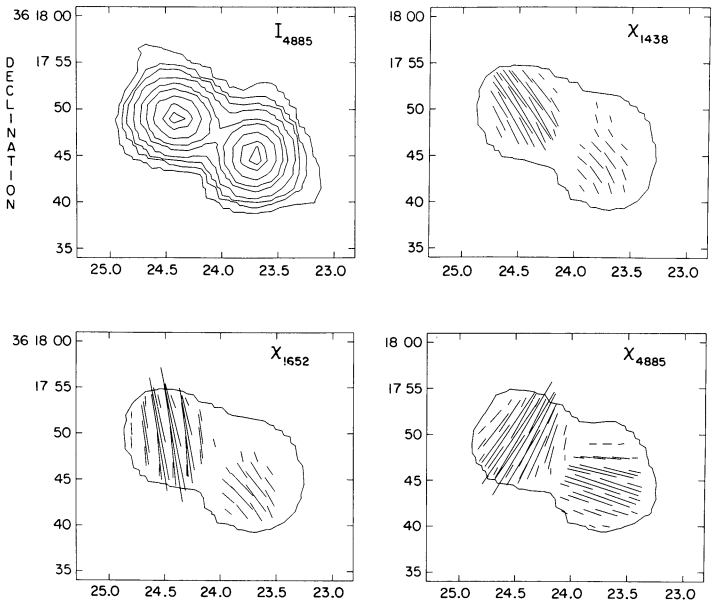

FIG. 2g

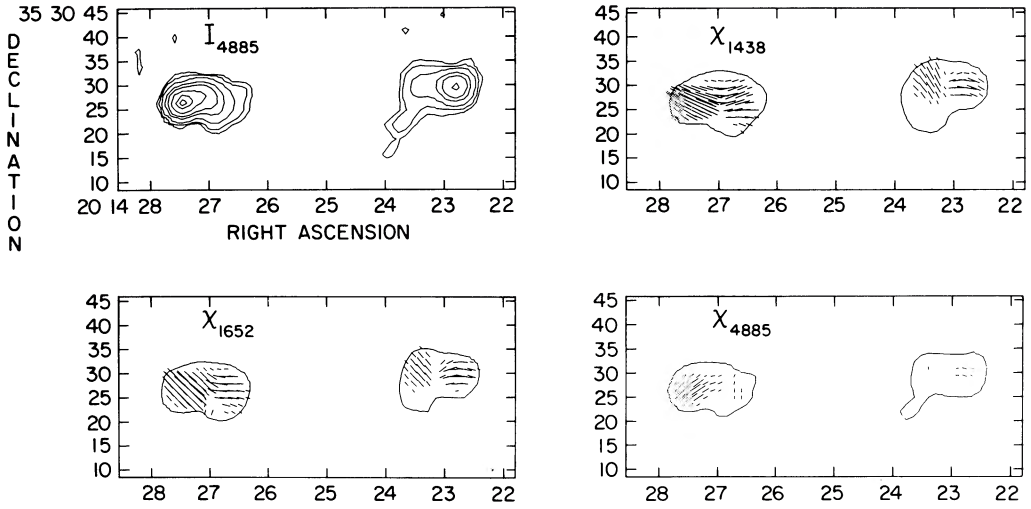

FIG. 2h

from the blank portions of the map, and therefore refers to the noise level of the map. The error in a portion of the map where a polarization signal is present is more difficult to measure, but in general will be greater than σ. These smaller errors will result in more constrained χ^2 measures of goodness of fit and might lead one to reject rotation measure values which are in fact appropriate.

As a result the errors in the measurement of the polarization position angles most likely lie somewhere between those of the averaging method and those of the single feature method. However, we find that the polarization position angles from the two methods agree reasonably well.

b) *Determination of the Rotation Measures and Rotation Measure Differences*

For each polarized source component, the rotation measure was determined by a least-squares fit of equation (1) to the measurements of polarization position angle ϕ at the four frequencies of observation. The goodness of fit was measured by the reduced chi-square, χ_r^2,

$$\chi_r^2 = \frac{1}{n_f} \sum_i \left(\frac{\phi_i - \psi_i'}{\sigma_{\phi_i}} \right)^2 , \tag{4}$$

where ϕ_i and σ_{ϕ_i} are the measured polarization position angle and its error, respectively, at the wavelength λ_i and n_f is the number of degrees of freedom. The angle ψ_i' is the model polarization position angle predicted for a rotation measure, RM, and corrected for an "$n\pi$ ambiguity,"

$$\psi_i' = \psi_i - n_i \pi \quad \text{with} \quad \psi_i = \phi_0 + \mathrm{RM}\lambda_i^2 , \tag{5}$$

where n_i is found by rounding the quantity $(\psi_i - \phi_i)/\pi$ to the nearest integer.

Extraction of unique rotation measures is complicated by the $n\pi$ ambiguity. It is well-known that in the case of polarization position angle measurements at two frequencies, there are an infinite number of rotation measures which can fit the observations. A polarization position angle measurement at a third frequency removes this ambiguity; but, in the presence of errors, nonuniqueness returns.

To combat such ambiguities, additional information which can constrain the rotation measure is necessary. One such constraint can be obtained from the depolarization. Extremely high values of the rotation measure lead to bandwidth depolarization. Rankin, Campbell, and Spangler (1975) have derived formulae for the depolarization as a function of rotation measure. We applied their formulae to determine, for each source, the maximum absolute rotation measure, $|\mathrm{RM}_{\mathrm{max}}|$, consistent with our measured values of depolarization. For all sources, $1000 < |\mathrm{RM}_{\mathrm{max}}| \lesssim 2500$ rad m^{-2}, with a mean value $|\mathrm{RM}_{\mathrm{max}}| \approx 1700$ rad m^{-2}. Since the observed depolarization is almost certainly not due exclusively to bandwidth effects, the derived upper limits are most likely overestimates. These limits were then used to exclude extremely large rotation measures.

Another such constraint is the polarization position angle difference between the two C bands, $\Delta\phi \equiv \phi_{4835} - \phi_{4885}$. As defined, $\Delta\phi$ has the same sign as RM, provided that there have been no $n\pi$ "wraps" between the two C bands. However, as the two C bands are separated by only 50 MHz, it would require a rotation measure of 4.5×10^4 rad m^{-2} for $\Delta\phi = \pi$. We may rule out any such rotation measures from depolarization considerations and confidently require that $\Delta\phi$ and RM have the same sign.

The mean $\Delta\phi$ for our sources is $0\overset{\circ}{.}5 \pm 0\overset{\circ}{.}3$, indicating that rotation measures in this portion of the sky are marginally more likely to be positive than negative. If we exclude the source 2014+355, which alone has large negative values for $\Delta\phi$, the mean value increases to $0\overset{\circ}{.}8 \pm 0\overset{\circ}{.}4$. These results indicate that, to 2 σ, the rotation measures in this portion of the sky are more often positive than negative.

This has two implications. First, it allowed us to narrow the range of rotation measures even further. The depolarization indicated the maximum of |RM|; the polarization position angle difference provided us with the sign. Second, these sources all lie within region A of Simard-Normandin and Kronberg (1980), a region they find to be characterized by predominately negative rotation measures. They attribute the negative rotation measures in region A to projection effects resulting from viewing sources along the large-scale galactic magnetic field. The indication that rotation measures in the Cygnus region are positive may signify that the magnetic field orientation in the Cygnus region is different than that of the Galaxy in this direction.

Even with the constraints on the rotation measure, the $n\pi$ ambiguity remained a problem. As an example of the presence and nature of the $n\pi$ "wrap" problem, we present our fit to the polarization position angle data of 2007+365 in Figure 3. This source had the lowest rotation measure among those sources in our sample for which we were able to determine the rotation measure. The solid lines represent good fits to the data. To emphasize the limitations on measuring polarization position angles, the solid lines have had an appropriate number of π "wraps" subtracted so that they remain within the region [0, π]. Clearly, the two L band frequencies are seen on different "wraps" of the polarization position angle.

A method of data display we found illuminating and which clearly illustrates the difference between the spatially averaged and single feature data is a plot of χ_r^2 as a function of RM. Figure 4 shows such plots for four features: one component of 2004+369, both components of 2007+365, and one component of 2014+355. The values of χ_r^2 were calculated using spatially averaged data for the north-preceding component of 2007+365 and the south-following component of 2014+355. For the other two components, single feature data were used.

The predominant feature of these plots is that, for certain rotation measures, the reduced chi-square drops to low values, indicating a good fit. As a rule of thumb, we adopted a $\chi_r^2 \leq 3.0$ as the criterion for a good fit. For two degrees of freedom, such a χ_r^2 corresponds to the 95% confidence level if polarization position angle errors are in a Gaussian distribution. Furthermore, due to the few degrees of freedom used in determining χ_r^2, we treated all values of RM for which $\chi_r^2 \leq 3.0$ as being equally preferable.

From Figure 4, we see that the only acceptable rotation measure for the north-preceding component of 2004+369 is about 800 rad m^{-2}. Similarly, for the south-following component of 2007+365, the only acceptable rotation measure is about 320 rad m^{-2}. However, for the north-preceding component of 2007+365 and the south-following component of 2014+355, using the spatially averaged estimates, a number of rotation measures are statistically permissible.

In general, the single feature method yielded fewer statistically acceptable rotation measures, due to the smaller errors associated with this method. Our suspicion that these errors were often underestimates was confirmed by the fact that for some of the components, no value of the RM produced

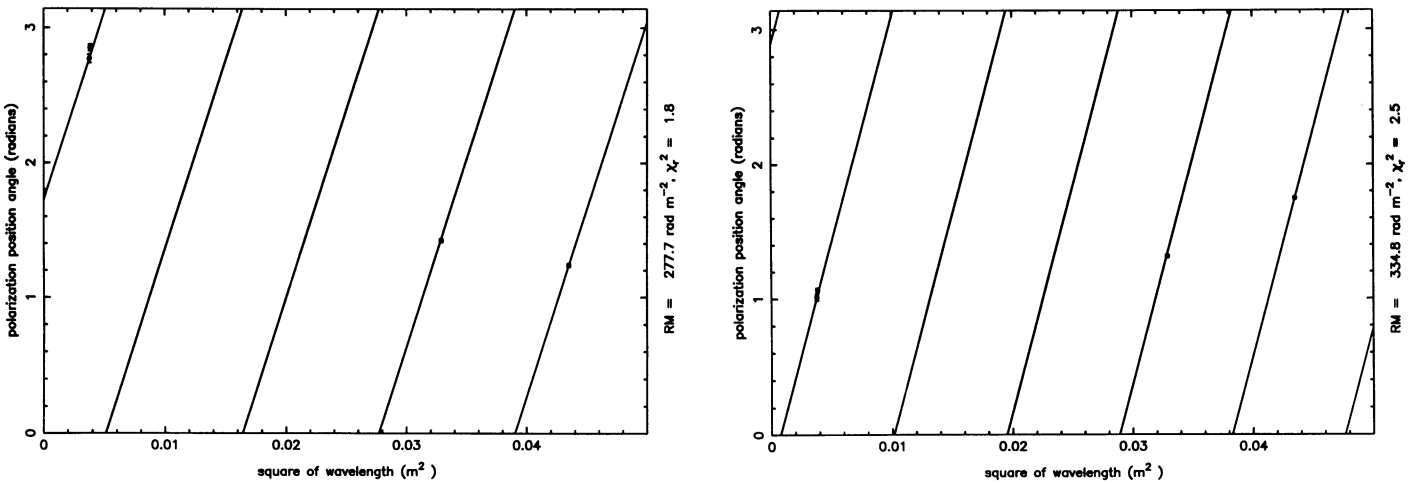

FIG. 3.—Polarization position angle as a function of the square of the wavelength showing good fits of the data. Shown are the north-preceding (*left panel*) and south-following (*right panel*) components of 2007 + 365, the source with the lowest rotation measure.

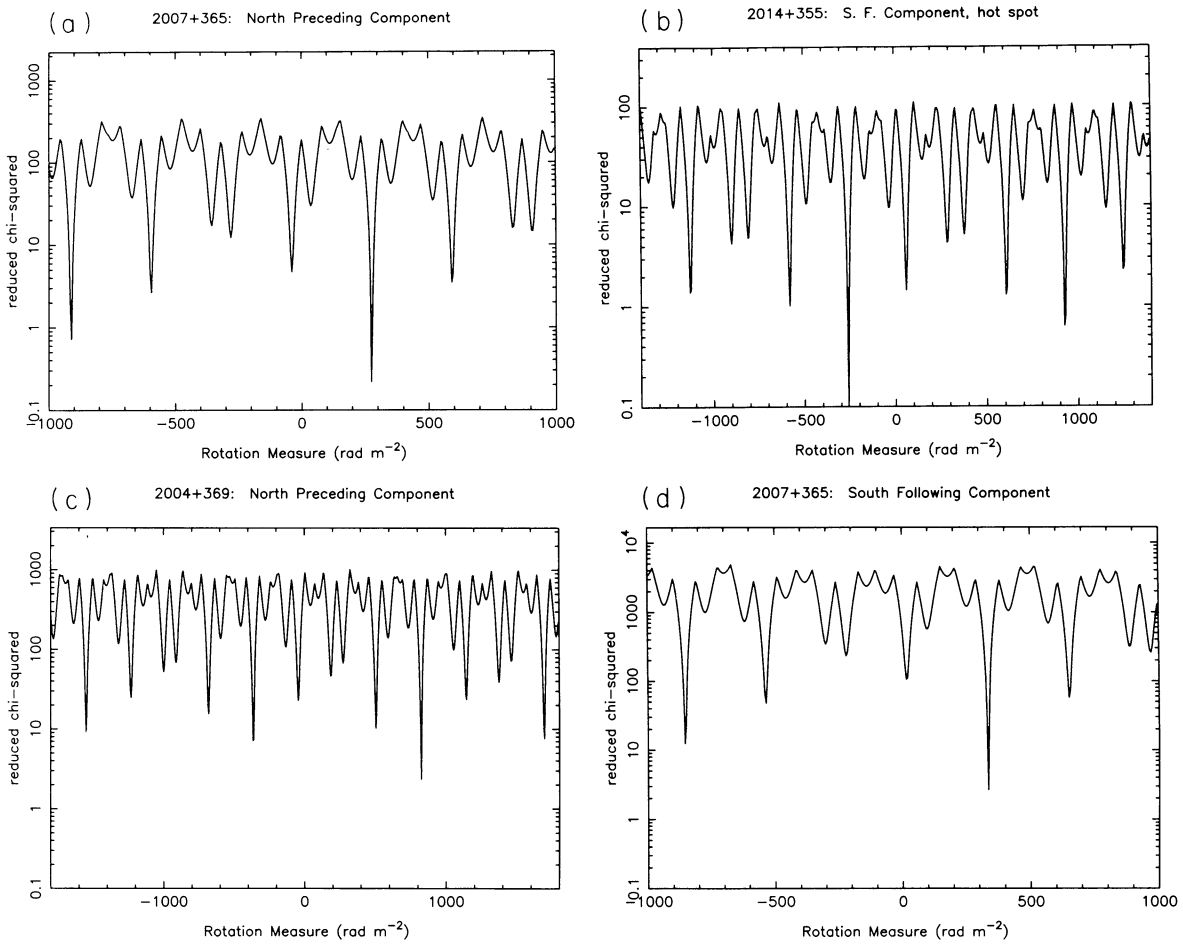

FIG. 4.—The reduced chi-square as a function of rotation measure. In (*a*) and (*b*), the north-preceding component of 2007 + 365 and the hot spot of the south-following component of 2014 + 355, respectively, are shown with the χ^2 having been calculated using spatially averaged data. Note that a number of rotation measures produce a $\chi_r^2 < 3.0$, our criterion for an acceptable fit. In (*c*) and (*d*), the north-preceding component of 2004 + 369 and the south-following component of 2007 + 365 are shown with the chi-squares having been calculated using single feature data. Note that in each case, only one rotation measure produces a $\chi_r^2 < 3.0$.

TABLE 3

UNAMBIGUOUS ROTATION MEASURES

Source	Component	RM (rad m^{-2})
2004+369.....	NP	822.7 (1.5)
	SF	850.5 (2.3)
2005+368.....	NP	693.7 (1.3)
	SF	690.0 (5.4)
2007+365.....	NP	277.7 (1.3)
	SF	334.80(0.92)
2011+360.....	SP	227.7 (1.7)
	NF	334.4 (2.2)

a χ_r^2 as small as 3, even though there were a few pronounced minima. We believe this situation indicates underestimates of the errors in the single feature method (as discussed above) rather than inadequacy of equation (1) to describe the frequency dependence of the position angle.

Due to the good agreement of the polarization position angles between the two methods, however, the minima occur at nearly the same rotation measure. This fact allowed us to reduce the number of possible rotation measures for many components. If the averaging method resulted in a great number of minima, the single feature results were examined. Rotation measures at which deep minima occurred in the single feature results were judged to be the most likely possibilities.

As a result of these analyses using the depolarization and the polarization position angle difference, we believe that we have determined the unambiguous rotation measures for four of the sources. Displayed in Table 3 is a list of the unambiguous rotation measures. In column (1) is the source, in column (2) is the component, and in column (3) is the rotation measure. All of the rotation measures given are found using single feature polarization position angles.

For the remaining three sources, we were unable to identify unambiguous rotation measures, in the sense that two or more rotation measures gave an equally good χ_r^2, for each source. However, in each case we were able to extract a *minimum* value for the rotation measure *difference* between components. Since the goal of this project is the construction of a rotation measure structure function, such rotation measure differences are actually the primary quantities of interest.

The minimum difference was calculated in a straightforward manner. For each component of an "ambiguous" source, a set of acceptable rotation measures was extracted. From these sets, all possible differences $|RM_1 - RM_2|$ were computed, and the minimum retained. It is worth pointing out that the sources for which we have reported an "unambiguous" rotation measure in Table 3 were also subject to the analysis for finding the minimum ΔRM. In each case, the minimum ΔRM corresponded to the difference of the values given in Table 3. The minimum ΔRM values therefore result from a consistent (and, we believe, robust) procedure applied to all the sources.

The rotation measure difference data are given in Table 4. Column (1) gives the source name, and column (2) gives the separation between the components in arcseconds. The many entries for 2014+355 result from the fact that this source has two polarized features in each component, and all possible differences are considered. Columns (3) and (4) give the minimum rotation measure difference, with the two columns containing the two different estimates. The values given in column (3) were calculated using rotation measures obtained from spatially averaged data, while the differences in column (4) were obtained from rotation measures using the brightest polarized feature data.

TABLE 4

MINIMUM VALUES FOR ΔRM

Source	$\Delta\theta$	Average ΔRM_{min} (rad m^{-2})	Feature ΔRM_{min} (rad m^{-2})
2003+383	11".6	69.6(7.1)	68.1(7.1)
2004+369	14.2	50.9(7.1)	27.8(7.1)[b]
2005+368	25.5	0.5(8.8)	3.7(7.1)[b]
2007+365	74.4	59.6(7.1)	57.1(7.1)
2011+360	45.9		106.7(7.1)[b]
2013+362	12.7	44.1(7.1)	35.2(7.1)[b]
2014+355[a]			
SF, h to SF, l	11.1	0.2(7.1)	0.2(7.1)[b]
SF, h to NP, h	70.1	52.7(7.1)	48.8(7.1)
SF, h to NP, l	61.0		44.4(7.1)
SF, l to NP, h	59.0	50.4(7.1)	48.6(7.1)[b]
SF, l to NP, l	50.0		44.2(7.1)[b]
NP, h to NP, l	9.3		4.4(7.1)

[a] Four polarized features were distinguished in this source: SF, h, south-following component, hot spot; SF, l, south-following component, lobe; NP, h, north-preceding component, hot spot; NP, l, north-preceding component, lobe.

[b] For one or both features, no RM produced a $\chi_\nu^2 \leq 3.0$.

We wish to emphasize the consistency of the results presented in Table 4. We obtain the same value for the minimum rotation measure difference between components, irrespective of using the spatial averaging or single feature method to obtain the polarization position angle and its error (whether we refer to col. [3] or [4] of Table 4). We saw above that the most intense feature method frequently indicated an "unambiguous" value of the rotation measure, whereas the spatial averaging method yielded only a set of possibilities. In spite of this quite different result regarding the absolute value of the rotation measure, the two techniques yield equivalent results for the rotation measure difference between components.

c) *The Sources*

We now discuss each of the eight sources in light of the measured rotation measures.

i) *2003+383*

Shown in Figure 2*a*, this source has a close double or core-jet structure, the two components being separated by approximately 11". The south-preceding component is substantially depolarized with the depolarization or ratio of the fractional linear polarization at the L bands to that at the C bands being 0.28. The north-following component is considerably less depolarized, the depolarization being 0.72. However, we were unable to extract the polarization position angle for the north-following component at 4835 MHz. This may have contributed to our inability to determine the rotation measures for this source. Examination of a reproduction of the Palomar Sky Survey print for this portion of the sky shows that this source is on the edge of a faint arc of emission which has a slightly fibrous appearance.

ii) *2004+369*

Another close double, this source is shown in Figure 2*b* and displays a number of features of interest. The amount of depo-

larization is moderate to small, being 0.5 to 0.7. The north-preceding component displays, at the two lower frequencies, resolved polarization position angle structure. Examination of the Palomar Sky Survey print shows that this source is also on an edge of an arc of emission, although this arc is considerably brighter than the one through which 2003+383 is viewed. In addition, numerous H II regions are on the line of sight to this object and two absorption nebulae lie nearby.

iii) *2005+368*

This double source is shown in Figure 2*c* and is more separated than the previous two with a separation of approximately 23″. The amount of depolarization, if present, is small for both components. Both components also display polarization structure at the lower frequencies, although the structure in the north-preceding component is not evident at the higher frequencies. In close proximity to 2004+369, this source is observed through the same arc of material. In contrast to 2004+369, however, 2005+368 lies well within the arc.

iv) *2007+365*

Shown in Figure 2*d*, this double with a separation of approximately 60″ has one of the largest separations in the group. It is also one of the weaker sources, yet polarization was detected at all frequencies with no evidence of depolarization. The polarization position angle is uniform across each component with no polarized emission detected in the bridge. Although not viewed through the same arc of emission as the two previous sources, 2007+365 does appear to lie either on the extreme outer edge of the arc or just outside of it. Nevertheless, some material still appears to be evident and a filament stretches from the arc toward 2007+365, terminating only a short distance from the source.

v) *2011+360*

A well-resolved double with a separation of approximately 40″, this source displays considerable polarization structure. As is seen in Figure 2*e*, both components have polarization structure which can be resolved at all four frequencies, with the north-following component displaying substantial changes in the polarization position angle across the feature. These changes are large enough to render the spatial averaging method inappropriate for this object. Both components also have moderate to little depolarization, with the fractional linear polarization ratio being between 0.5 to 0.7. This source lies on or just to the side of a filament of optical emission.

vi) *2012+388*

As this source is unpolarized at the lower frequencies, Figure 2*f* shows only the total intensity contour image and the 4885 MHz polarization position angle image. The source lies very near a bright region on the Palomar Sky Survey print. The line of sight intersects or passes near numerous H II regions. Due to lack of polarized emission at the low frequencies, this source was excluded from any of the analyses.

vii) *2013+362*

This close double has a separation of approximately 11″ and is shown in Figure 2*g*. The depolarization is considerable, being less than 0.4 for both components. There is some evidence for resolvable polarization structure, but in general the polarization position angle is uniform across each component. This source lies not far from the terminus of the filament on which 2011+360 is located. The region surrounding the line of sight for this source has less prominent optical emission than many of the other lines of sight, however, some faint emission can be seen.

viii) *2014+355*

With components separated by approximately 60″, this double is one of the more widely separated sources in our sample. As can be seen from Figure 2*h*, four distinct areas, two per component, of polarized emission are present at all four frequencies. However, there are insufficient data at 4885 MHz for the lobe of the north-preceding component to employ the spatial averaging method. Nevertheless, with the single feature method, it is possible to use these four areas to determine changes in the rotation measure within components. The separation between features of polarized emission within components is approximately 10″. Depolarization, if present, is small. This source is viewed through a region of comparatively little optical emission. The rotation measure differences stated for 2014+355 deserve additional comment. There are two sets of rotation measures (≈ -300 rad m^{-2} and ≈ 900 rad m^{-2}) which produce deep minima and equivalent rotation measure differences using either spatially averaged or single feature data. It is possible, using spatially averaged data, to find a smaller rotation measure difference. However, this difference is between one of the deep minima and a much more shallow minimum. Therefore, we consider it probable that the larger difference, presented in Table 4, is in fact correct.

V. THE ROTATION MEASURE STRUCTURE FUNCTION

Having found the rotation measures and/or rotation measure differences for seven of the eight sources, we wish to use them to form the structure function given by equation (3). However, in practice we cannot obtain equation (3) with our limited number of measurements. The process of taking an expectation value implies averaging an infinite number of independent measurements with the same $\Delta\theta$. To construct a reasonable facsimile of the rotation measure structure function would require a major expansion of our data set. Our present measurements can only give us an estimate of the rotation measure differences on different scales, which can be compared with model estimates to see if the observed differences are of the same order as the model.

In Figure 5, we plot the squares of our RM differences as a function of the angular separation. The data with separations ($\Delta\theta$) of 10″–20″ represent either polarized features within the same component of a source or components of the closely spaced doubles. More widely separated doubles are indicated by the data with $\Delta\theta$ between 30″ and 100″. These intrasource differences are taken from Table 3 for sources possessing unambiguous rotation measures and from Table 4 for the remaining sources. Intersource rotation measure differences are indicated by the data with $\Delta\theta$ greater than 1000″; here we are utilizing the data in Table 3. In all cases, we have utilized rotation measures obtained from single feature data.

We note two features of Figure 5 which indicate that the Faraday rotation measure fluctuations are of interstellar, rather than intrinsic, origin. First, the typical rotation measure differences between components, of order 30 to 50 rad m^{-2} for $\Delta\theta \leq 100''$, are considerably greater than those observed for similar sources at high galactic latitudes. Simard-Normandin, Kronberg, and Button (1981), Simonetti, Cordes, and Spangler (1984), and Leahy (1987) all show that for similar radio sources at high galactic latitudes, absolute rotation measures are an order of magnitude smaller than for our sources and intra-

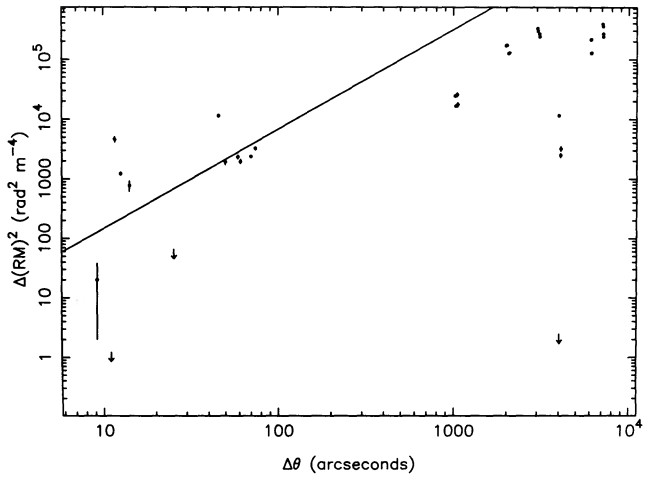

FIG. 5.—The estimate of the rotation measure structure function: data are taken from Table 3 for those sources with unambiguous rotation measures and from Table 4 for sources with ambiguous rotation measures. The sloping straight line is that of eq. (6).

source rotation measure differences are a few radians m^{-2} or less. The second argument in favor of an interstellar origin of the rotation measure fluctuations is that the value of the structure function increases with increasing angular separation, $\Delta\theta$. This is quite comprehensible if the fluctuations arise in the interstellar medium (ISM), since more widely separated lines of sight are probing different spatial scales; whereas if the rotation measures were intrinsic, there should be no dependence on the separation of the lines of sight.

Having argued that the structure function in Figure 5 arises from interstellar plasma turbulence, we next ask what we would expect for such a relationship, given our knowledge about such turbulence. The simplest model for the rotation measure fluctuations is one in which it is assumed that the density fluctuations responsible for the scattering have no associated magnetic field variation. This is almost certainly physically incorrect; the magnetohydrodynamic equations couple these quantities together and, except in extreme cases, a variation in one will engender a variation in the other. Nonetheless, we might conjecture that this physically incorrect model will correctly predict the magnitude and spectral characteristics of rotation measure fluctuations within a factor of 2 or so. The appealing feature of this model is that rotation measure variations may be directly related to scattering measurements. We stress that we do not consider this a satisfactory final description of matters. Even so, this model might be sufficient to indicate if the ISM density fluctuations are broad-band in nature or confined to a narrow spectral range.

Given this simple model for the interstellar density turbulence, Simonetti and Cordes (1988) have obtained the following expression for the expected rotation measure structure function:

$$D_{\rm RM}(\Delta\theta) = (2.89 \times 10^5)(C_n^2 L)\langle B_\parallel\rangle^2 (L\Delta\theta)^{(5/3)} . \quad (6)$$

Here $\Delta\theta$ is the angular separation in degrees between the lines of sight probed, $\langle B_\parallel\rangle$ is the systematic component of the line of sight magnetic field strength in microgauss, and L is the path length through the turbulent medium in kiloparsecs. This expression assumes a Kolmogorov spectrum of density irregularities. All the parameters on the right-hand side are known with the exception of L, which may be reasonably estimated. The product $C_n^2 L$ is exactly the quantity determined in angular broadening measurements. Spangler *et al.* (1986) have determined this quantity to be 0.18 $m^{-(20/3)}$ kpc for lines of sight very close to the sources of interest. A good estimate for the value of the systematic component of the interstellar magnetic field is 4 μG (Heiles 1987). Since in the Cygnus region we are looking approximately along the systematic field, uncertainty in the projection angle is minimized. Finally, we estimate the thickness of the region containing the turbulence to be about 2 kpc (Bochkarev and Sitnik 1985). This parameter is the most poorly known in equation (6).

Given these input quantities, equation (6) yields the relationship indicated by the solid line in Figure 5. Despite the crudeness of the model for the turbulence (density fluctuations with no corresponding magnetic field perturbation) and uncertainty in the thickness of the medium, this is a remarkable reconstruction of the observations. Recall that this line is a *prediction* based on the scattering measurements, and not a fit with floating parameters whose values are otherwise unconstrained. The curve reproduces the rotation measure differences for angular separations less than a few hundred arcseconds, although it appears to overshoot the data on the several degree scale.

There is no question that there is great latitude in fitting these (still admittedly sparse) measurements. For example, one could attempt to fit all the data with a single power law of a more shallow slope. We feel, however, the most remarkable result is that the extrapolated curve in Figure 5 produces the correct magnitude for rotation measure differences. It is worth emphasizing the vast range in spatial scale over which the extrapolation has occurred. The angular separations of 10″–100″ displayed in Figure 5 correspond, for an assumed distance to the turbulent layer of 1–2 kpc, to scales of 10^{17}–10^{18} cm. The turbulence responsible for angular broadening in this region (Spangler and Cordes 1988), on the other hand, occurs on spatial scales of 10^8–10^9 cm. The clear indication of Figure 5 is then that the same power-law spectrum spans a range of nine orders of magnitude in spatial scale. This, together with the recent results by Cordes *et al.* (1989) for the pulsar 1937+214, suggests that the density spectrum in the intense scattering regions is indeed a Kolmogorov-like power law with a large inertial subrange.

VI. RESULTS AND CONCLUSIONS

The results of this paper are as follows:

1. We have discovered eight extragalactic radio sources viewed through the galactic plane in the region of Cygnus and close to the Cygnus OB 1 association. These sources may be suitable as probes of the interstellar medium for other types of investigations, such as H I absorption.

2. Linear polarization observations have been made at frequencies of 1438, 1652, 4835, and 4885 MHz. Least-squares fits to the polarization position angle data have allowed us to extract unambiguous rotation measures for four of the eight sources. These rotation measures range from +230 to +853 rad m^{-2}.

3. The positive rotation measures observed for these sources are in contrast with the rotation measures of a large majority of sources in region A (Simard-Normandin and Kronberg 1980), indicating that the magnetoionic component of the ISM has highly localized structure.

4. For three of the remaining four sources as well as the preceding four, we have obtained measurements of the

minimum rotation measure difference between polarized components of the sources. The rotation measure differences range from less than a few rad m^{-2} to 105 rad m^{-2}. We observe roughly 50–100 rad m^{-2} difference for features separated by 30″–60″.

5. An observational facsimile to the rotation measure structure function has been obtained by plotting the square of the rotation measure difference between the two polarized components of a source versus the angular separation between these components. The squares of the rotation measure differences are larger than typically observed for similar sources, similarly observed, at high galactic latitudes. We furthermore observe $(\Delta RM)^2$ increasing with angular separation between components. These two observed properties lead us to attribute these RM fluctuations to the interstellar medium.

6. The observed rotation measure differences are in quite good quantitative agreement with the expected differences if the spectrum of density irregularities measured by interstellar scattering in this region extends to scale sizes of order 10^{18} cm. The interstellar scattering observations are sensitive to fluctuations on scales of 10^8–10^9 cm.

7. The plasma density power spectrum in intense scattering regions is a quasi-Kolmogorov power law extending over approximately nine to ten orders of magnitude. This result should have considerable significance for theories on the generation of these irregularities.

We wish to thank J. D. Fix, L. A. Molnar, and A. Clegg for helpful discussions. This research was supported at the University of Iowa by grants NAGW-806 and NAGW-831 from the National Aeronautics and Space Administration. At Cornell University, we were supported by the Alfred P. Sloan Foundation, grant AST-8520530 from the National Science Foundation, and the National Astronomy and Ionosphere Center. T. J. L. was supported in part by the Undergraduate Scholar Assistantship program at the University of Iowa.

REFERENCES

Armstrong, J. W., Cordes, J. M., and Rickett, B. J. 1981, *Nature*, **291**, 561.
Bochkarev, N. G., and Sitnik, T. G. 1985, *Ap. Space Sci.*, **108**, 237.
Cordes, J. M., Rickett, B. J., and Backer, D. C., eds. 1988, *AIP Conf. Proc. No. 174, Radio Wave Scattering in the Interstellar Medium* (New York: AIP).
Cordes, J. M., Weisberg, J. M., and Boriakoff, V. 1985, *Ap. J.*, **228**, 221.
Cordes, J. M., Wolszczan, A., Dewey, R. J., Blaskiewicz, M., and Stinebring, D. R. 1989, *Ap. J.*, **349**, 245.
Dennison, B., Thomas, M., Booth, R. S., Brown, R. L., Broderick, J. J., and Condon, J. J. 1984, *Astr. Ap.*, **135**, 199.
Fey, A. L., Spangler, S. R., and Mutel, R. L. 1989, *Ap. J.*, **337**, 730.
Heiles, C. 1987, in *Interstellar Processes*, ed. D. Hollenbach and H. Thronson (Dordrecht: Reidel), p. 171.
Higdon, J. C. 1984, *Ap. J.*, **285**, 109.
———. 1986, *Ap. J.*, **309**, 342.
Leahy, J. P. 1987, *M.N.R.A.S.*, **226**, 433.
Lee, L. C., and Jokipii, J. R. 1976, *Ap. J.*, **206**, 735.
Montgomery, D., Brown, M. R., and Matthaeus, W. H. 1987, *J. Geophys. Res.*, **92**, 282.
Rankin, J. M., Campbell, D. B., and Spangler, S. R. 1975, *National Astronomy and Ionosphere Center Report 46*.
Simard-Normandin, M., and Kronberg, P. P. 1980, *Ap. J.*, **242**, 74.
Simard-Normandin, M., Kronberg, P. P., and Button, S. 1981, *Ap. J. Suppl.*, **45**, 97.
Simonetti, J. H., and Cordes, J. M. 1988, in *AIP Conf. Proc. No. 174, Radio Wave Scattering in the Interstellar Medium*, ed. J. M. Cordes, B. J. Rickett, and D. C. Backer (New York: AIP), p. 134.
Simonetti, J. H., Cordes, J. M., and Spangler, S. R. 1984, *Ap. J.*, **284**, 126.
Spangler, S. R. 1988, in *AIP Conf. Proc. No. 174, Radio Wave Scattering in the Interstellar Medium*, ed. J. M. Cordes, B. J. Rickett, and D. C. Backer (New York: AIP), p.66.
Spangler, S. R., and Cordes, J. M. 1988, *Ap. J.*, **332**, 346.
Spangler, S. R., Mutel, R. L., Benson, J. M., and Cordes, J. M. 1986, *Ap. J.*, **301**, 312.

James M. Cordes and T. Joseph Lazio: Department of Astronomy, Space Sciences Building, Cornell University, Ithaca, NY 14853

Steven R. Spangler: Department of Physics and Astronomy, Van Allen Hall, University of Iowa, Iowa City, IA 52245